Received 4 September 1997; accepted 10 September 1998.

1. Morgan, J. W. Convection plumes in the lower mantle. *Nature* **230,** 42–43 (1971).
2. Olson, P., Schubert, G. & Anderson, C. Plume formation in the D″-layer and the roughness of the core-mantle boundary. *Nature* **327,** 409–413 (1987).
3. Wolfe, C. J., Bjarnason, I. T., VanDecar, J. C. & Solomon, S. C. Seismic structure of the Iceland mantle plume. *Nature* **385,** 245–247 (1997).
4. Nataf, H.-C. & VanDecar, J. C. Seismological detection of a mantle plume? *Nature* **264,** 115–120 (1993).
5. Wen, L. & Helmberger, D. V. A 2D P-SV hybrid method and its applciation to modeling localized structures near the core-mantle boundary. *J. Geophys. Res.* **103,** 17901–17918 (1998).
6. Kind, R. & Müller, G. Computations of SV waves in realistic earth models. *J. Geophys. Res.* **41,** 149–172 (1975).
7. Garnero, E. J., Grand, S. P. & Helmberger, D. V. Low *P*-wave velocity at the base of the mantle. *Geophys. Res. Lett.* **20,** 1843–1846 (1993).
8. Garnero, E. J. & Helmberger, D. V. Seismic detection of a thin laterally varying boundary layer at the base of the mantle beneath the central Pacific. *Geophys. Res. Lett.* **23,** 977–980 (1996).
9. Liu, X.-F. & Dziewonski, A. M. Lowermost mantle shear wave velocity structure (abstr.) *Eos* **75,** 663 (1994).
10. Schweitzer, J. & Müller, G. Anomalous difference travel times and amplitude ratios of SKS and SKKS from Tonga-Fiji events. *Geophys. Res. Lett.* **13,** 1529–1532 (1986).
11. Garnero, E. J. & Helmberger, D. V. A very slow basal layer underlying large-scale low-velocity anomalies in the lower mantle beneath the Pacific: evidence from core phases. *Phys. Earth Planet. Inter.* **91,** 161–176 (1995).
12. Garnero, E. J. & Helmberger, D. V. Further structural constraints and uncertainties of a thin laterally varying ultralow-velocity layer at the base of the mantle. *J. Geophys. Res* **103,** 12495–12509 (1998).
13. Helmberger, D. V., Zhao, L.-S. & Garnero, E. J. in *Seismic Modeling of the Earth Structure* (eds Boschi, E., Ekstrom, G. & Morelli, A.) 183–222 (North-Holland, New York, 1996).
14. Helmberger, D. V., Garnero, E. J. & Ding, X. Modeling two-dimensional structure at the core-mantle boundary. *J. Geophys. Res.* **101,** 13963–13972 (1996).
15. Helmberger, D. V., Wen, L. & Ding, X. Extremes in CMB structure beneath Europe and Africa. *Eos* **78,** 46 (1997).
16. Jeanloz, R. & Garnero, E. J. Interpretation of D″ and the core-mantle boundary region. *Eos* **78,** 46 (1997).
17. Mori, J. & Helmberger, D. V. Localized boundary layer below the mid-Pacific velocity anomaly identified from a P_CP precursor. *J. Geophys. Res.* **100,** 20359–20365 (1995).
18. Revenaugh, J. & Meyer, R. Seismic evidence of partial melt within a possibly ubiquitous low-velocity layer at the base of the mantle. *Science* **277,** 670–673 (1997).
19. Vidale, J. E. & Hedlin, M. A. Intense scattering at the core-mantle boundary north of Tonga: evidence for partial melt. *Nature* **391,** 682–684 (1998).
20. Wen, L. & Helmberger, D. V. Ultra-low velocity zones near the core-mantle boundary from broadband PKP precursors. *Science* **279,** 1701–1703 (1998).
21. Williams, Q. & Garnero, E. J. Seismic evidence for partial melt at the base of Earth's mantle. *Science* **273,** 1528–1530 (1996).
22. Holland, K. G. & Ahrens, T. J. Melting of $(Mg,Fe)_2SiO_4$ at the core-mantle boundary of the Earth. *Science* **275,** 1623–1625 (1997).
23. Shen, Y., Soloman, S., Bjarnason, I. T. & Purdy, G. Hot mantle transition zone beneath Iceland and the adjacent mid-Atlantic Ridge inferred from P-to-S conversions at the 410- and 660-km discontinuities. *Geophys. Res. Lett.* **23,** 3527–3530 (1996).
24. Williams, Q., Revenaugh, J. & Garnero, E. J. A correlation between the hot spot distribution and ultra-low basal velcocities in the mantle. *Science* **281,** 549–564 (1998).
25. Dziewonski, A. M. & Anderson, D. L. Preliminary reference earth model (PREM). *Phys. Earth Planet. Inter.* **25,** 297–356 (1981).
26. Grand, S. P., van der Hilst, R. D. & Widiyantoro, S. Global seismic tomography: A snapshot of convection in the Earth. *GSA Today* **7,** 1–7 (1997).

Acknowledgements. We thank J. Ritsema for comments on early drafts. This work was supported by the NSF.

Correspondence and requests for materials should be addressed to D.V.H. (e-mail: helm@gps.caltech.edu).

Seismic evidence for small-scale dynamics in the lowermost mantle at the root of the Hawaiian hotspot

Sara A. Russell*, Thorne Lay* & Edward J. Garnero†

* *Earth Sciences Department, University of California, Santa Cruz, California 95064, USA*

† *Seismological Laboratory, University of California, Berkeley, California 94720, USA*

The hot thermal boundary layer produced by heat transport from the Earth's core to the base of the mantle is thought to contain strong horizontal shear flows and to nucleate instabilities in which hot material rises into the convecting mantle as thermal plumes[1–3]. A recent study[4,5] proposes that the Hawaiian plume is deflected by mantle convection and, in the lowermost mantle, is located to the southeast of its surface manifestation. Here we present seismic data that densely sample, with core-reflected shear waves, a region beneath the central Pacific Ocean which includes the predicted location of the deflected root of the Hawaiian hotspot. Our mapping of the structure in this region of the lowermost mantle reveals strong lateral gradients in shear-wave velocity and anisotropic shear-wave polarization direction over distances of only several hundred kilometres. We interpret these gradients as being indicative of small-scale dynamical structure in the thermal boundary layer, where vertical flow into the Hawaiian plume at its root is accompanied by horizontal flow towards the plume.

We examine shear waves traversing the deep mantle below a region southeast of Hawaii from 54 earthquakes in the Tonga–Fiji region recorded on 34 digital broadband seismometers in western North America (Fig. 1a). This data set provides better spatial resolution than any other study of deep mantle anisotropy[6] because most previous studies used phases that diffract for long distances along the core–mantle boundary (CMB) and had less dense station distributions.

We analyse shear-wave reflections from the CMB at epicentral distances of 73° to 84° as these provide the best possible spatial sampling of deep mantle structure in our study area. Shallow mantle effects are suppressed by considering ScS differential times relative to the direct S phase (Fig. 1b), which turns at shallower depths in the mantle, and by applying corrections for models of anisotropic lithospheric structure beneath the receivers[7,8]. For the travel-time analysis we use the tangential components of motion (ScSH and SH), as these are free of complexities due to the core-traversing, longitudinally polarized SKS phase in our distance range. The ScS polarization on the tangential and longitudinal (ScSV) components is investigated in the shear-wave splitting analysis.

The central Pacific area studied is known to have anomalous shear-velocity structure in the lowermost mantle. Several global seismic tomography models indicate that our study area has slower-than-average shear velocity, in contrast to faster-than-average velocities characterizing regions beneath margins of the Pacific Ocean[9–12]. A shear-velocity model, M1, with a 3% velocity reduction in the lowermost 200–300 km of the mantle has been proposed for this region[13], and there is compelling evidence for a layer (~10 km thick) above the CMB with strongly reduced velocities (5–10% decreases for P-wave velocity and 15–30% for S-wave velocity)[14–17]. The low shear velocities are likely to indicate hotter than average temperatures, with the very large velocity reductions at the base of the boundary layer suggesting partial melt[18]. Seismic anisotropy, manifested by shear-wave splitting, may result from mineralogical or structural alignments that reflect the strain and/or stress regime in a given region[6,7,19]. Anisotropy with SH faster than SV has been found to the northeast of our study area, and mixed or negligible anisotropy closer to our region[20,21].

Our shear-wave signals are selected to be simple and impulsive to minimize the uncertainties involved in measuring arrival times. Using the cleanest arrival onsets and peaks, we measure differential times between ScSH and SH for a subset of 248 out of 762 seismograms. The differential travel times average 4 s larger than predicted by the reference velocity model PREM[22], much of which can be accounted for by model M1[13]. We find a strong lateral gradient in the differential times anomalies increasing towards the northeast with respect to PREM (Fig. 2a). The ray-path geometry is such that this low-velocity structure need not be strictly confined to the base of the mantle, although absolute travel times indicate that ScS is the phase responsible for the differential behaviour. 3.5% lateral variations in shear velocity in the lowermost 250 km of the mantle over length scales of 600 km can account for the 4 s increase in ScS delay across our study region. Confining the anomalous zone to the lowermost 100 km of the mantle requires extreme lateral gradients of 7% over 300-km scale lengths. Conversely, distributing the anomalous structure over greater depth extent towards the northeast from the CMB reflection points in Fig. 2a allows reduction of the magnitude of the velocity decrease. Although the geometry of the heterogeneous structure is not uniquely resolved, our data clearly sample a low-shear-velocity region with strong lateral gradients involving velocities that decrease in the northeasterly direction.

In addition, shear-wave splitting measurements were made for the 81 ScS observations that are most free of contamination from S and SKS arrivals. The splitting delays between the fast and slow polarizations are typically of the order of 1.0 s, with values as large as 2.0 s, after correction for lithospheric anisotropy and a small phase shift (~0.2 s at 78°) of ScSV at the CMB. The directions of the fast polarization angles are plotted at the ScS reflection points in Fig. 2b. The data have significant scatter; however, estimates of the polarization direction are expected to be very unstable for small values of splitting delay (the lengths of the arrows in Fig. 2b are proportional to the splitting delay).

In the northeast portion of the study area, the larger splitting values are generally oriented in the along-path direction (from southwest to northeast), indicating that ScSV arrives earlier than ScSH. In the southwest, the larger splitting times are associated with fast directions in a nearly orthogonal direction (that is, ScSH travels faster than ScSV). This rotation of polarization is unlikely to be an artefact created by the lithospheric corrections as individual stations yield a wide range of splitting angles for rays that arrive at

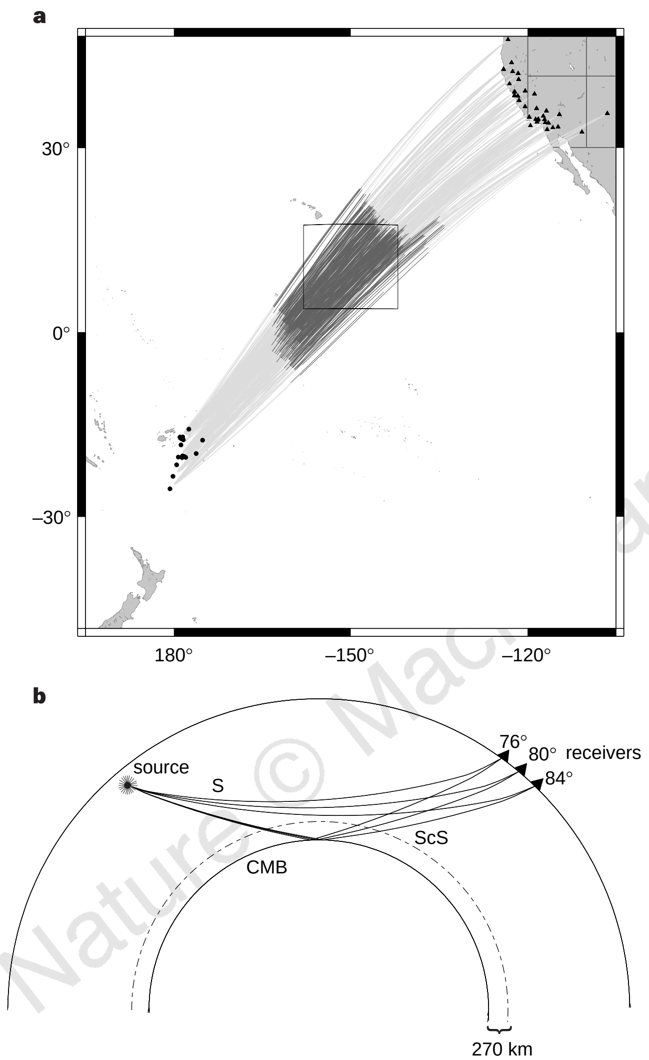

Figure 1 Geometry of ray-paths. Ray diagrams showing the ray-paths between the earthquake sources (magnitudes > 5.1, depths 250–650 km) in Tonga–Fiji and the digital broadband stations in the Berkeley Digital Seismic Network, Caltech USGS/TERRAscope and the IRIS (Incorporated Research Institutions for Seismology) seismic arrays. **a**, Surface projection of the ray-paths with the dark grey lines southeast of Hawaii indicating where ScS traverses the lowermost 270 km of the mantle. The box marks the region at the core–mantle boundary (CMB) encompassing the ScS reflection points. **b**, S and ScS ray-paths computed for model M1[13] for a source at a depth of 500 km at epicentral distances of 74°, 80° and 84°. The direct S wave turns in the mid-mantle while ScS reflects off the CMB. The dominant periods of our observations are ~10 s and the associated Fresnel zone at the CMB (the spatial extent sampled by the finite frequency reflection) is an ellipse elongated along the ray-path direction with principle axis dimensions of about 5° by 10°. The direct S phase is used as a reference to ScS to cancel common effects on their similar paths through the upper mantle. A comparison of absolute S and ScS travel-time anomalies with the ScS-S anomalies reveals that the ScS anomalies have a relatively stronger correlation. This indicates that ScS encounters anomalous low-velocity structure in the deep mantle where the ray-path separates from S.

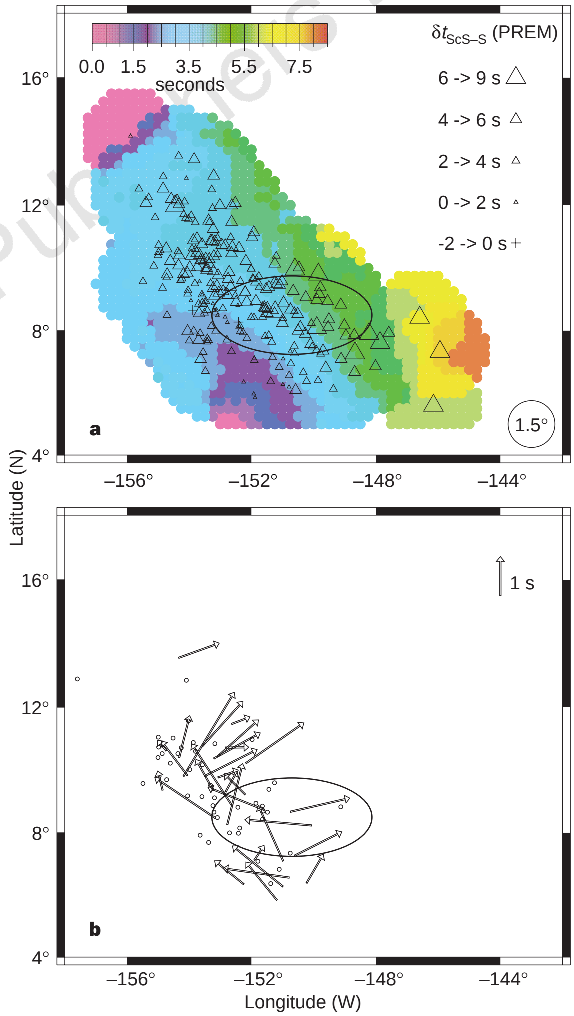

Figure 2 Map views of the travel-time residuals and anisotropy measurements plotted at the ScS CMB reflection points. **a**, Travel-time residuals $((ScSH - SH)_{obs} - (ScS - S)_{PREM})$ smoothed with a gaussian cap-average with cap radius of 1.5°. The colour scale is for the cap-average values. The ellipse represents the predicted location of the root of the Hawaiian plume based on mantle convection models. **b**, ScS fast polarization directions and splitting magnitudes plotted at their CMB reflections points. The arrows point in the direction of the fast component, as measured from north, and the length of the arrow indicates the magnitude of split. The circles represent data that either were too noisy to obtain a reliable measurement or did not possess any measurable splitting. There is a 0.4-s uncertainty in the splitting magnitudes and a 23° uncertainty in the polarization direction, based on the inverse F test[28]. A transition appears from fast directions perpendicular to the ray-paths in the southwest to fast directions parallel to the ray-paths in the northeast. The ellipse is the same as in **a**.

approximately the same incidence angle and with azimuths varying by less than 7°. There is no intrinsic requirement that the quasi-shear wave polarizations be related to the great-circle reference frame, but the few intermediate polarization directions found are mostly for observations with weak splitting. Figure 3 illustrates representative waveforms in the great-circle coordinate system, as well as the optimal fast/slow quasi-shear wave coordinate system, with the clear time offset of ScSV and ScSH almost coinciding with the optimal splitting.

This bimodal behaviour shows the simplest spatial pattern, segregating arrivals with different polarization directions, when the measurements are projected to the ScS turning points, shown in Fig. 2b. There is much more mingling of direction when the data are plotted at intersections with shallower depth surfaces. Shear-wave-splitting observations for direct S phases that traverse the deep mantle to the northeast of our study area show intermittent cases of fast SH or fast SV as well as no onset-time splitting[21,23], suggesting that shear-wave splitting does not accumulate systematically with path length towards the northeast. These factors favour an interpretation of strong lateral variation in anisotropy on lateral scale lengths of 300–500 km within the lowermost mantle. Lateral gradients of 2–3% in the velocity ratio v_{SH}/v_{SV}, and 90° changes in the fast polarization direction over scale lengths of 500 km, are required if we confine the variations to the thermal boundary layer at the CMB. As these are sub-Fresnel-zone scale lengths, it is difficult to constrain the actual structure, but Fig. 2 provides a strong case for coupled lateral gradients in shear velocity (with ScSH slowing relative to SH towards the northeast) and anisotropy (with ScSH slowing relative to ScSV towards the northeast). This gradient occurs near the postulated origin of the Hawaiian plume.

Although there are several viable mechanisms, sheared chemical heterogeneities or partial melt zones appear to be the leading candidates for producing seismic anisotropy near the base of the mantle[6,24]. Sheared melt inclusions can efficiently induce shear-wave anisotropy, even with small melt fractions[25]. In circum-Pacific regions, which contain higher than average shear velocities and anisotropy with $v_{SH} > v_{SV}$, several studies have suggested that down-welling oceanic slab structures, possibly involving partial melt or chemical heterogeneities within the slab, contribute to the anisotropy[25,26]. As our study area is far from zones of historic subduction, slabs are probably not involved. Given the presence of a very low velocity zone right at the base of the mantle that appears to involve partial melt[18,27], and the overall low velocity structure in the region, the most likely explanation for our observations involves strong shear-flow-induced fabrics with inclusions of partial melt and/or chemical heterogeneity.

Lateral shear flows within the CMB boundary layer are likely to horizontally shear partial melt inclusions and to develop chemically distinct lamellae (Fig. 4). This can explain the observations in the southwestern portion of our study area of the relatively fast ScSH arrival (although still slow in an absolute sense). In the northeastern portion of the study area, a transition to vertical flow would create general anisotropy with vertical striations or lamellae of partial melt in the medium, allowing ScSV to travel faster than ScSH. It is likely that partial melt distributions are concentrated towards the CMB and, to the extent that this concentrates anisotropic structure towards the CMB, the magnitude of the anisotropy should increase with depth. Are such small-scale gradients common, as might be expected within a chaotic, unstable boundary layer, or are we seeing an extreme case due to the large magnitude of the expected

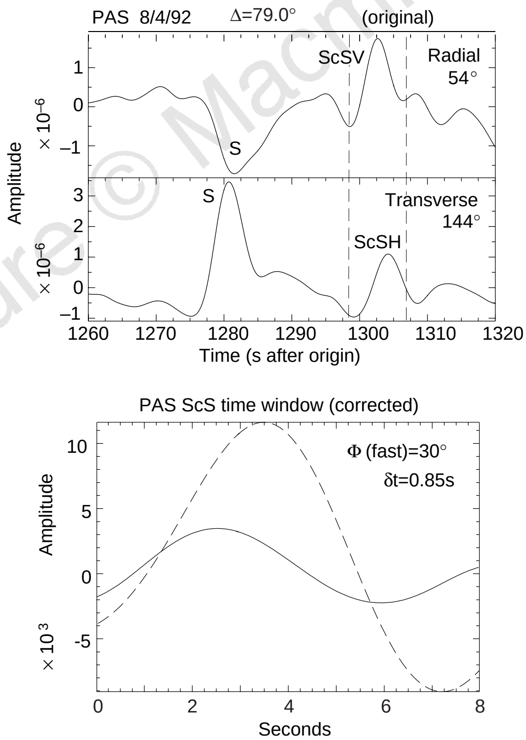

Figure 3 Two seismograms from different events and stations which illustrate the presence of variable anisotropy across our study region. The upper panels show the uncorrected radial and transverse components of the S and ScS phases. The vertical lines denote the time window of the signals in the lower panel. The lower panels are the windowed corrected integrated ScS phases rotated to the fast/slow polarization direction Φ (fast component shown by the solid line). Corrections for known lithospheric anisotropy were applied using parameters derived from S and SKS splitting measurements in previous studies[7]. The ScS angles of emergence are close to those of the SKS waves so the corrections are appropriate. A small correction that varies with epicentral distance, ~0.2 s, was also applied for the phase shift of ScSV on reflection from the CMB relative to ScSH. The corrected data were cross-correlated to seek a linear polarization of the ScS motion as a function of fast polarization angle and splitting delay[7,8]. A covariance method[28] to find the splitting parameters was also utilized and the values plotted are those obtained in both procedures. Standard particle motion and confidence region plots were also generated to confirm the reliability of these results[28].

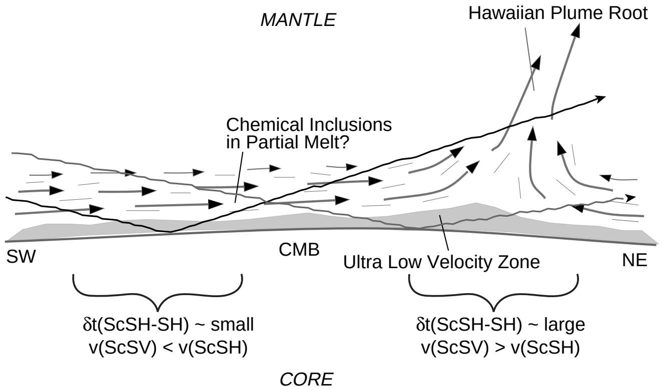

Figure 4 A cartoon of the boundary layer at the CMB that incorporates the differential travel time and anisotropy observations. Differential shear flows that upwell into a mantle plume in the northeast affect ray paths differently depending on what region they sample. ScS reflecting in the southwestern region (left) would have ScSH travel faster than ScSV due to the horizontally sheared structure with embedded partial melt, while in the northeastern region (right) ScSV will travel faster than ScSH due to vertically sheared fabric of partial melt and chemical heterogeneity. The transition from lateral to vertical structure would impart different anisotropic splitting to the two ray-paths.

boundary layer inflow feeding the Hawaiian plume? The strong gradients in structure at the boundary layer revealed in our data support the presence of small-scale dynamics at the CMB. As this has many implications for heat transport and interactions between the core and mantle, further comparable high-resolution investigations of other regions are necessary to explore this dynamical regime. □

Received 12 December 1997; accepted 1 September 1998.

1. Stacey, F. D. & Loper, D. E. The thermal boundary layer interpretation of D″ and its role as a plume source. *Phys. Earth Planet. Inter.* **33,** 45–55 (1983).
2. Sleep, N. H. Hotspots and mantle plumes: Some phenomenology. *J. Geophys. Res.* **95,** 6715–6736 (1990).
3. Loper, D. E. & Lay, T. The core-mantle boundary region. *J. Geophys. Res.* **100,** 6397–6420 (1995).
4. Steinberger, B. M. *Motion of Hotspots and Changes of the Earth's Rotation Axis Caused by a Convecting Mantle.* Thesis, Harvard Univ. (1996).
5. Steinberger, B. & O'Connell, R. J. Advection of plumes in mantle flow: Implications for hotspot motion, mantle viscosity and plume distribution. *Geophys. J. Int.* **132,** 412–434 (1998).
6. Lay, T., Garnero, E. J., Williams, Q., Kellogg, L. & Wysession, M. E. in *The Core-Mantle Boundary* (eds Gurnis, M., Buffett, B. A., Knittle, E. & Wysession, M.) 299–318 (Geodynamics Ser., Vol. 28, Am. Geophys. Union, Washington DC, 1998).
7. Silver, P. G. Seismic anisotropy beneath the continents: Probing the depths of geology. *Annu. Rev. Earth Planet. Sci.* **24,** 385–432 (1996).
8. Ansel, V. & Nataf, H.-C. Anisotropy beneath 9 stations of the GEOSCOPE broadband network as deduced from shear-wave splitting. *Geophys. Res. Lett.* **16,** 409–412 (1989).
9. Su, W.-J., Woodward, R. & Dziewonski, A. M. Degree 12 model of shear velocity heterogeneity in the mantle. *J. Geophys. Res.* **99,** 6945–6980 (1994).
10. Li, X. D. & Romanowicz, B. Global mantle shear velocity model developed using nonlinear asymptotic coupling theory. *J. Geophys. Res.* **101,** 22245–22272 (1996).
11. Masters, T. G., Johnson, S., Laske, G. & Bolton, H. A shear-velocity model of the mantle. *Phil. Trans. R. Soc. Lond. A* **354,** 1385–1411 (1996).
12. Grand, S. P., van der Hilst, R. D. & Widiyantoro, S. Global seismic tomography: A snapshot of convection in the Earth. *GSA Today* **7,** 1–7 (1997).
13. Ritsema, J., Garnero, E. & Lay, T. A strongly negative shear velocity gradient and lateral variability in the lowermost mantle beneath the Pacific. *J. Geophys. Res.* **102,** 20395–20411 (1997).
14. Revenaugh, J. S. & Meyer, R. Seismic evidence of partial melt within a possibly ubiquitous low velocity layer at the base of the mantle. *Science* **277,** 670–673 (1997).
15. Vidale, J. E. & Hedlin, M. A. H. Evidence for partial melt at the core-mantle boundary north of Tonga from the strong scattering of seismic waves. *Nature* **319,** 682–685 (1998).
16. Mori, J. & Helmberger, D. V. Localized boundary layer below the mid-Pacific velocity anomaly identified from a PcP precursor. *J. Geophys. Res.* **100,** 20359–20365 (1995).
17. Garnero, E. J. & Helmberger, D. V. Seismic detection of a thin laterally varying boundary layer at the base of the mantle beneath the central-Pacific. *Geophys. Res. Lett.* **23,** 977–980 (1996).
18. Williams, Q. & Garnero, E. J. Seismic evidence for partial melt at the base of Earth's mantle. *Science* **273,** 1528–1530 (1996).
19. Karato, S.-I. in *Rheology of Solids and of the Earth* (eds Karato, S. & Toriumi, M.) 393–422 (Oxford Univ. Press, 1989).
20. Vinnik, L., Romanowicz, B., Le Stunff, Y. & Makeyeva, L. Seismic anisotropy in the D″ layer. *Geophys. Res. Lett.* **22,** 1657–1660 (1995).
21. Ritsema, J., Lay, T., Garnero, E. & Benz, H. Seismic anisotropy in the lowermost mantle beneath the Pacific. *Geophys. Res. Lett.* **25,** 1229–1232 (1998).
22. Dziewonski, A. M. & Anderson, D. L. Preliminary reference earth model. *Phys. Earth Planet. Inter.* **25,** 297–356 (1981).
23. Pulliam, J. & Sen, M. K. Seismic anisotropy in the core-mantle transition zone. *Geophys. J. Int.* (in the press).
24. Lay, T., Williams, Q. & Garnero, E. J. The core-mantle boundary layer and deep earth dynamics. *Nature* **392,** 461–468 (1998).
25. Kendall, J.-M. & Silver, P. G. Constraints from seismic anisotropy on the nature of the lowermost mantle. *Nature* **381,** 409–412 (1996).
26. Matzel, E., Sen, M. K. & Grand, S. P. Evidence for anisotropy in the deep mantle beneath Alaska. *Geophys. Res. Lett.* **23,** 2417–2420 (1996).
27. Holland, K. G. & Ahrens, T. J. Melting of $(Mg,Fe)_2SiO_4$ at the core-mantle boundary of the Earth. *Science* **275,** 1623–1625 (1997).
28. Silver, P. G. & Chan, W. W. Shear wave splitting and subcontinental mantle deformation. *J. Geophys. Res.* **96,** 16429–16454 (1991).

Acknowledgements. We thank B. Steinberger for providing a preprint and details of his calculations for the Hawaiian hotspot, and R. Hartog for providing several codes for measuring anisotropy. Data were obtained through the IRIS, BDSN and TERRAscope data centres. This work was supported by the US NSF.

Correspondence and requests for materials should be addressed to S.R. (e-mail:sara@earthsci.ucsc.edu).

Sauropod dinosaur embryos from the Late Cretaceous of Patagonia

Luis M. Chiappe*, Rodolfo A. Coria†, Lowell Dingus‡, Frankie Jackson§, Anusuya Chinsamy‖¶ & Marilyn Fox#

* *Department of Ornithology, American Museum of Natural History, Central Park West at 79th Street, New York, New York 10024, USA*
† *Museo Municipal 'Carmen Funes', 8318 Plaza Huincul, Neuquén, Argentina*
‡ *Department of Vertebrate Paleontology, American Museum of Natural History, Central Park West at 79th Street, New York, New York 10024, USA*
§ *Department of Paleontology, Museum of the Rockies, Montana State University, Bozeman, Montana 59717, USA*
‖ *Zoology Department, University of Cape Town, Private Bag, Rondebosch 7700, South Africa*
¶ *South African Museum, PO Box 81, Cape Town 8000, South Africa*
\# *Department of Vertebrate Paleontology, Peabody Museum of Natural History, Yale University, New Haven, Connecticut 06520, USA*

Definitive non-avian dinosaur embryos, those contained inside fossil eggs, are rare[1,2]. Here we describe the first known unequivocal embryonic remains of sauropod dinosaurs—the only known non-avian dinosaur embryos from Gondwana—from a nesting ground in the Upper Cretaceous stage of Patagonia, Argentina. At this new site, Auca Mahuevo (Fig. 1), thousands of eggs are distributed over an area greater than 1 km^2. The proportion of eggs containing embryonic remains is high: over a dozen *in situ* eggs and nearly 40 egg fragments encasing embryonic material were recovered. In addition to bone, these specimens contain large patches of fossil skin casts, the first definitive portions of integument ever reported for a non-avian dinosaur embryo. As morphology of the eggs enclosing these osseous and integumentary remains is identical, we propose that these specimens belong to the same sauropod species. This discovery allows the confident association of the megaloolithid type of dinosaur eggshell[3] with sauropod dinosaurs.

Embryonic bone is typically found flattened on the bottom of the egg. Only the shafts of postcranial elements are preserved in the Auca Mahuevo specimens prepared so far, and few cranial elements are easily identifiable from a mass of diagenetically fused bone. Nevertheless, cranial remains from two specimens (PVPH-112 and PVPH-113) allow a confident taxonomic identification of these embryos. Loose, pencil-like teeth are distinct (Fig. 2). PVPH-112 has at least 32 teeth, with one complete tooth measuring 2.0 mm. The teeth have straight margins that gradually taper towards the crown's apex. Crowns are formed by smooth enamel that lacks denticles or primary ridges. The absence of crown denticles is considered to be a synapomorphy of neosauropods[4] (these include the common ancestor of *Saltasaurus* and *Diplodocus* plus all its descendants[4,5]). Among dinosaurs, pencil-like teeth are known from diplodocid, dicreaosaurid and titanosaur neosauropods[4]. The